Citation
Li, Z. and Chen, W. and Hao, H. 2018. Numerical study of sandwich panel with a new bi-directional Load-Self-Cancelling (LSC) core under blast loading. Thin-Walled Structures. 127: pp. 90-101. http://doi.org/10.1016/j.tws.2018.02.003

Numerical study of sandwich panel with a new bi-directional Load-Self-Cancelling (LSC) core under blast loading

Zhejian Li, Wensu Chen*, Hong Hao*

Centre for Infrastructural Monitoring and Protection

School of Civil and Mechanical Engineering, Curtin University, Australia

**Corresponding author*

Abstract

A new form of bi-directional Load-Self-Cancelling (LSC) sandwich panel is proposed in this paper. An array of square dome shaped steel sheet as core of the proposed sandwich panel is designed to cancel a certain amount of load during blast event owing to its arching geometry. The blast resistance and energy absorption capabilities of the sandwich panel are investigated numerically by using finite element analysis software LS-DYNA. The peak deflection of centre point on back face sheet, internal energy and peak boundary reaction forces are compared among monolithic plate, multi-arch uni-directional LSC structure, sphere dome structure and the proposed bi-directional LSC square dome sandwich panel. It is found that using the proposed bi-directional LSC square dome leads to 69%, 48% and 56% reduction in the out-of-plane boundary reaction force as compared to the other three structures, respectively. In addition, parametric studies of the influences of dome number, height, and layer material on the performances of the proposed bi-directional LSC sandwich panel subjected blast loads of different intensities are carried out to investigate the panel configuration on the effectiveness of its blast resistance and load-self-cancelling capability. The results demonstrate the superiority of the sandwich panel with the proposed bi-directional LSC core.

Keywords: Bi-directional; Load-Self-Cancelling; Blast loads; Sandwich panel; Numerical study

1. Introduction

Accidental explosion and terrorism activities have been increasing around the globe in recent years, and more than half of which were related to bombing attacks [1-3]. As a protection of life and infrastructure from bomb attack, blast resistant panels have been widely used across military, commercial and industrial applications [4-6]. Blast-resistant doors as an example of such panels are used at entrances of shelters and ammunition storage magazines. The traditional blast resistant doors are often designed as a solid panel of great weight which leads to poor operational performance and high costs [7]. The ideal characteristics of a blast resistant panel should be lightweight while capable of resisting blast loads.

Various blast resistant panels have been developed. Due to the lightweight and high energy absorption capability, different sandwich structures which consist of a relatively thick and lightweight core sandwiched by two thin skin layers, have been proposed to absorb energy in recent years [8]. The performances of sandwich structures with different forms, materials and topologies have been comprehensively reviewed [9-11]. Forms of sandwich structure core usually include honeycomb, corrugate, metallic foam, lattice and functionally graded core. Superior performance of sandwich structures under dynamic loading has been demonstrated via both numerical simulations and experimental tests [12-19]. Other forms of structures such as egg-box, negative Poisson's ratio, and continuously graded lattice structure were investigated for their energy absorption performance under dynamic loading [20-24]. Curved sandwich panel with aluminium foam as core also demonstrated superior performance over equivalent flat sandwich panel and solid plate against blast loading [25-28]. Most of the previous studies focused on the energy absorption and the deformation of the panel after blast, the investigations on blast load transferred to the supports were limited. In practice, supports of the structural panel also need be properly designed and protected because damage to the support may lead to the complete failure of the panel structure. In this regard, a uni-directional multi-arch panel was proposed [7, 29]. This innovative design makes use of the unique property of arch structure form that transfers a certain amount of load applying onto the arch to the supports. In this case loads in the opposite directions at the intersections of adjacent arches would cancel each other, leading to reductions of the net loads to the supports of the structural panel. Both numerical simulations and experimental tests verified the effectiveness of the uni-directional multi-arch panel in resisting blast and impact loads [7, 29]. However, some limitations of using this uni-directional panel were also identified. It cancels loads only in one direction therefore its effectiveness in load-cancellation is effective in one direction only. Detailed discussions on the designs and performances of uni-directional multi-arch panels subjected to blast and impact loads can be found in the references [7, 29, 30].

To overcome the shortcomings of the uni-directional multi-arched panel, a bi-directional LSC sandwich structure is proposed in this study, the core consists of an array of two-axis-symmetric square domes as shown in Figure 1. This new structural form is believed having capability of cancelling load in both in-plane directions of the panel and therefore further reducing forces that would be transferred to the panel boundaries as compared to the uni-directional multi-arch panel. With the geometry similar to the proposed bi-directional LSC square dome structure, a modified structure named as “grid dome” is also numerically simulated in this study for comparison. It was originally proposed in [31], where the textile composite material and half sphere shape made it easy to deform and absorb energy. The grid of half spheres are placed with gaps between each other in the panel [31]. The array of grid sphere is modified and placed next to each other in this study to make it similar to the bi-directional LSC structure proposed in this study, since the load can be cancelled at the intersection points of the adjacent sphere domes as well. However, the adjacent grids of sphere domes are only point connected while the proposed square dome structure are connected with intersection lines, which allow more forces to be self-cancelled. Therefore, a superior LSC capacity is expected for the proposed square dome structure.

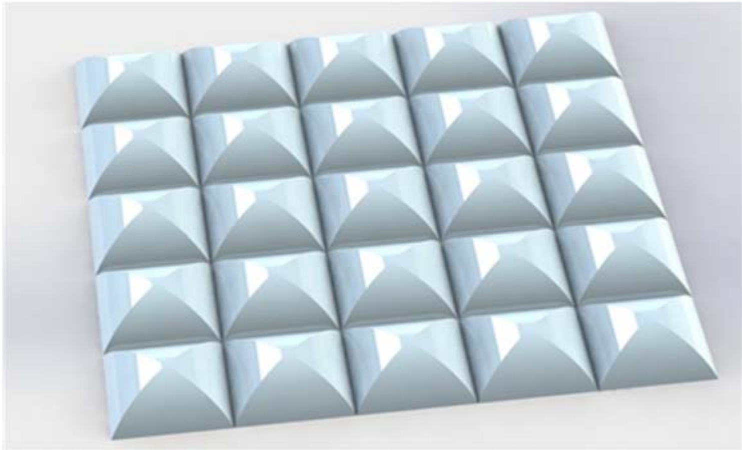

Figure 1. Proposed square dome as core of bi-directional load-self-cancelling structure

In this study, the effectiveness of this new form of LSC structure is numerically investigated and compared with an equivalent monolithic plate, and a uni-directional multi-arch structure [7] and a modified grid sphere dome structure [31]. Finite element software LS-DYNA 971 is employed in this study to calculate and analyse energy absorption, back plate centre deflection and boundary reaction forces of these structures under blast loading. The existing blast test data of a flat plate from other researchers is used to calibrate the numerical model. To validate the numerical model, the numerical results of dynamic response of the flat plate are compared with the existing experimental data. The calibrated numerical model is then used to perform numerical simulations of the proposed structure to evaluate its energy absorption capacity, blast load resistance capacity and boundary reaction forces. A series of parametric studies are also conducted to investigate the effectiveness of sandwich panels with different core configurations on their blast loading resistance capacities.

2. Numerical Model Calibration

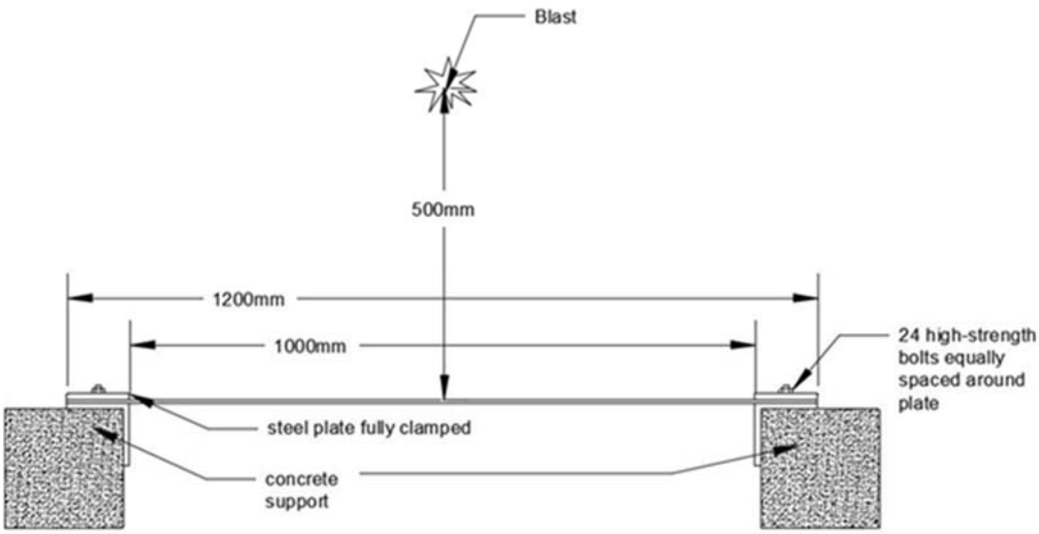

Figure 2. Experimental setup of a steel plate subjected to blast load

Finite element software LS-DYNA 971 is used for numerical simulation in this study. As a widely applied FEA tool based on explicit numerical methods, LS-DYNA is dedicated to highly nonlinear, dynamic finite element analysis subjected to impact and blast loads. To calibrate the accuracy and reliability of the numerical model, a steel plate which was tested and numerically modelled by DSTO (Defence Science and Technology Organization) of Australia is adopted [32]. In year 2000, a series of blast tests were carried out to study structural response of a 5 mm thick mild steel plate. The charges of 250 g Pentolite (260 g TNT equivalent [7]) were applied with the alternating stand-off distance of 250 mm, 400 mm, 500 mm directly above the centre of the steel plate with dimension of 1200 mm by 1200 mm. The steel plates were bolted on to a 1000 mm by 1000 mm rigid steel frame with 24 equally spaced high-strength bolts. The steel frame was simply supported by concrete stands on four sides with some openings. The schematic diagram of experimental setup of the steel plate is shown in Figure 2. Two accelerometers, pressure gauges and a LVDT displacement gauge were attached on the steel plate to record relevant data of the plate during and after the explosion. The test results are used to calibrate the numerical model in this study.

2.1 Element, mesh convergence test and boundary condition

The numerical model is constructed in Solidworks and LS-Prepost. The steel plate is modelled by using the fully integrated shell element to minimize hourglass energy in following simulations [33]. As an important factor for determining both the computational time and simulation accuracy, mesh size convergence tests are carried out with the element sizes of 20 mm, 10 mm, 5 mm, and 2.5 mm. Mesh convergence test results are shown and discussed in section 2.4.

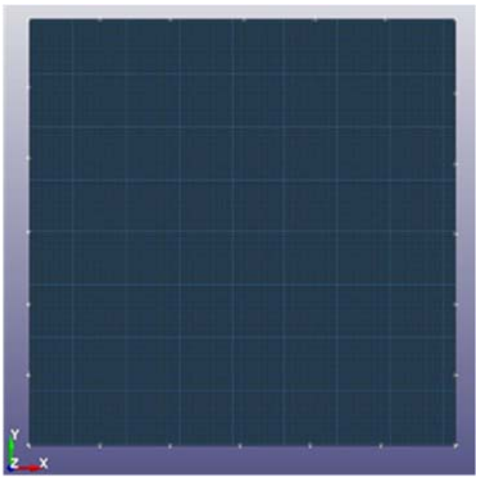

Figure 3. Boundary condition for finite element model of bolted steel plate subjected to blast loading

Boundary condition can be another critical factor for numerical simulation. In the model calibration and mesh convergence test, a simplified boundary condition for this steel plate subjected to blast loading is used to reduce computational time while representing the test conditions as closely as possible. In the simplified boundary condition, as shown in Figure 3, 24 nodes are modelled as fully fixed to represent the 24 bolts that connected the steel plate and steel frame in the test, other nodes along the plate edges are constrained in three degrees of freedom, UZ, Rot X and Rot Y by using *BOUNDARY SPC SET. This simplified approach was also adopted in Chen and Hao [7], and showed relatively good agreement with the test data.

2.2 Material model used in LS-DYNA

Table 1. Material properties of steel plate in Cowper and Symonds model [32]

Property	**Young's modulus (GPa)**	**Poisson's ratio**	**Yield stress (MPa)**	**Tangent modulus (MPa)**	**Density (kg/m3)**	**Hardening parameter, β**	C **(s^{-1})**	P
Value	203	0.3	270	470	7850	1	40	6

The elastic-plastic material model *MAT 003 PLASTIC KINEMATIC is adopted for modelling the steel plate. This material model is commonly used for modelling metals with bi-linear elastic-plastic constitutive relationship and isotropic or kinematic hardening plasticity which is defined by a hardening parameter β. Here β equals to 1, representing isotropic hardening, is used. Material strain rate effect is also considered by applying Cowper-Symonds model in LS-DYNA which is defined by Eq. (1) [33] .

$$\frac{\sigma_d}{\sigma_s} = 1 + \left(\frac{\dot{\varepsilon}}{C}\right)^{\frac{1}{p}} \tag{1}$$

where σ_d is the dynamic yield stress at plastic strain rate $\dot{\varepsilon}$, σ_s is the static yield stress. Strain rate parameters C and P are Cowper and Symonds constants, respectively. Material properties of steel used in this study are shown in Table 1. Failure strain of steel material is taken as 0.3 throughout this study.

2.3 Blast load modelling

*LOAD BLAST ENHANCED via the CONWEP feature in LS-DYNA is used to simulate blast load in numerical simulation [34]. The enhancement of reflected waves in blast event is demonstrated in the blast model. Pressures on the plate are determined by the amount of TNT, standoff distance and incident angle as given in the equation (2) below:

$$P(\tau) = P_r cos^2\theta + P_i(1 + cos^2\theta - 2cos\theta) \quad (2)$$

where P_r is the reflected pressure, P_i is the incident pressure and θ is the angle of incidence. The keyword *LOAD BLAST SEGMENT in LS-DYNA is applied to define the loading face of the structure and the keyword *DATABASE BINARY BLSTFOR is used to export the blast pressure data. The scaled distance is defined by equation:

$$Z = \frac{R}{W^{\frac{1}{3}}} \quad (3)$$

where R is the standoff distance in meter and W is the equivalent amount of TNT in kg.

2.4 Results and discussions of numerical model validation and mesh convergence test

Table 2. Experimental and numerical results of peak reflected pressure and peak displacement

Event	**TNT equivalent (g)**	**Standoff (mm)**	**Experiment data [32]**		**Numerical simulation**			
			P_r (MPa)	δ_{max} (mm)	P_r (MPa)	Error	δ_{max} (mm)	Error
E14	260	500	9.4	-33	9.3	1.0%	-31.2	5.4%
E16	260	400	16.4	-36	15.7	4.3%	-33.4	7.2%
E17	260	250	40.0	-35	44.5	-11.3%	-33.5	4.3%

The calculated reflected pressure-time histories from explosion at stand-off distances of 250 mm, 400 mm and 500 mm are shown in Figure 4. Numerical simulation results obtained using the model with mesh size of 5 mm and the experimental data under the same loading conditions are compared as listed in Table 2. The centre point peak displacement (δ_{max}) and the peak blast reflected pressure (P_r) of the three different stand-off distances are compared and a good agreement between the test data and numerical results is observed.

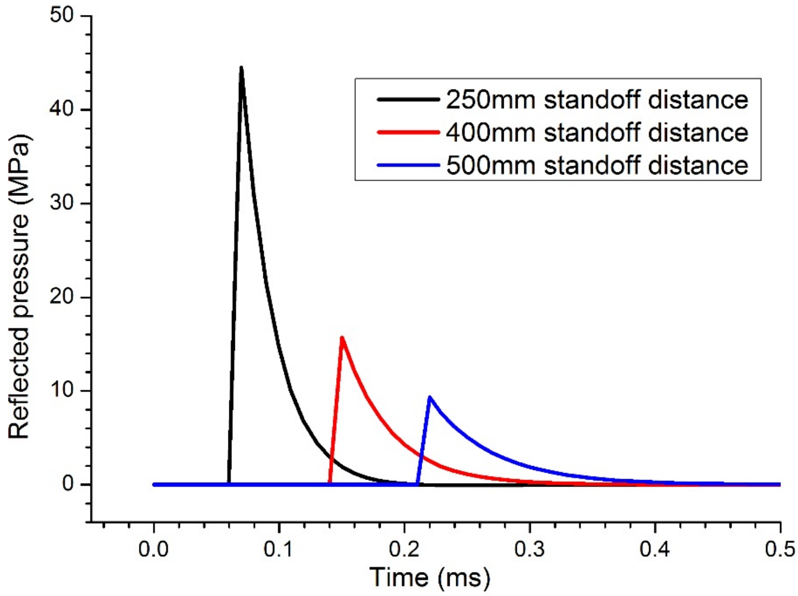

Figure 4. Reflected pressure time histories of steel plates with 250 mm, 400 mm and 500 mm stand-off distances

The results of mesh convergence test are shown in Figure 5. The discrepancy between the results corresponding to the mesh size of 20 mm from the rest are obvious while the results for the mesh size of 10 mm, 5 mm and 2.5 mm are close. It can be concluded that using the mesh size of 10 mm leads to reasonable numerical simulations as compared to the smaller mesh sizes, while the calculation on the model with finer mesh takes a substantially longer time. Therefore, the mesh size of 10 mm is acceptable. However, many structures simulated in this study contain different curvatures such as square dome, sphere dome, using 10 mm mesh leads to certain loss of geometry details. Therefore, 5 mm mesh size is employed in the subsequent analysis to ensure simulation accuracy and a reasonable computational time.

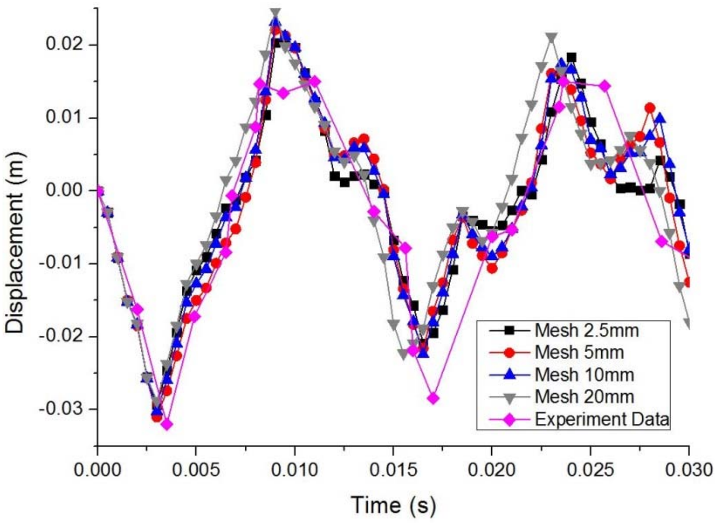

Figure 5. Displacement time histories with different mesh sizes and experimental data from event 14 [32]

3. Numerical Simulations

The calibrated numerical model is used to perform simulations of dynamic response of monolithic plate, uni-directional LSC multi-arch sandwich panel, sphere dome sandwich structure and the proposed bi-directional LSC square dome sandwich panel under blast loading. The structural response quantities, i.e., the peak deflection at the centre of back plate, energy absorption and peak boundary reaction forces, are calculated and compared to evaluate their blast resistant performance.

3.1 Panel configuration

A flat plate with the size of 1000 mm by 1000 mm and the thickness of 5 mm is employed for comparison with the uni-directional and bi-directional LSC sandwich structures. The core of uni-directional LSC sandwich panel (A5) consists of five arches with the same length, width and arch height of 50 mm (H50) as shown in Figure 6. The proposed bi-directional LSC structure consists of five square domes along each horizontal direction (D5), with 25 domes in total. Each dome is 200 mm in length and width, 50 mm in arch height (H50). The whole panel has the size of 1000 mm by 1000 mm. As shown in Figure 7 the modified grid dome panel configuration is similar to that of the square dome panel, consisting of five sphere domes along each in-plane direction. Each dome has a 200 mm diameter and 50 mm height. Uni-directional LSC multi-arch, grid sphere dome and bi-directional LSC square dome sandwich structures have a 2 mm-thick top plate and a flat sheet attached at back with a thickness of 1.5 mm. The thickness of the core varies for each example in order to keep the overall mass of the panel the same. The schematic diagram of bi-directional LSC panel is shown in Figure 8. The interfaces between the core and the skins are treated as welded.

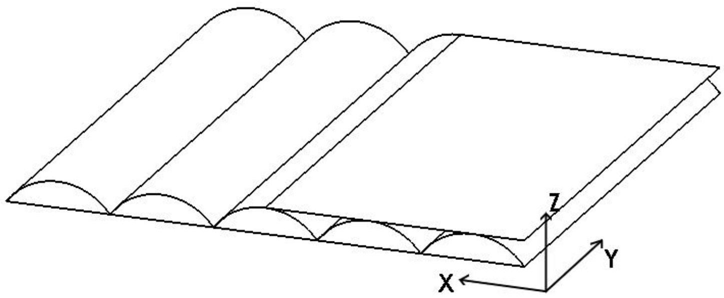

Figure 6. Five-arch uni-directional LSC sandwich panel with half of top plate removed for illustration.

Figure 7. Grid sphere dome sandwich structure with top plate partially removed for illustration.

Four panels i.e. flat plate (F1), uni-directional LSC multi-arch panel (A5-H50), grid sphere dome panel (S5-H50) and bi-directional LSC square dome panel (D5-H50) are analysed and the results are compared in the subsequent sections. Parametric simulations are presented in Section 4 to investigate the influences of size, geometry, material and loading condition of the square dome panel on its blast resistance capacity.

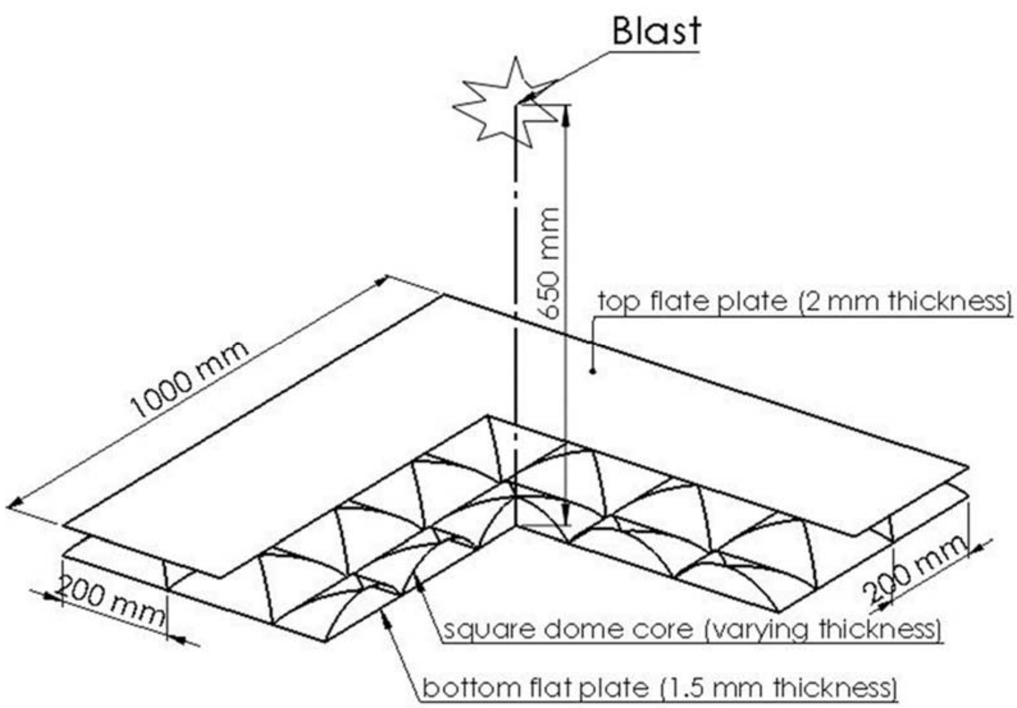

Figure 8. Schematic diagram of bi-directional LSC sandwich structure with five square domes in each direction

3.2 Finite element modelling

The fully integrated shell element with mesh size of 5 mm is used for numerical simulations. Boundaries of back plate of the panels are assumed to be fully fixed by constraining the nodes on four edges of the back flat plate in six degrees of freedom. The top face sheet and core are not constrained. Welded connection is applied for all the interfaces between layers using tied contact. The blast load applying onto the front flat sheet is simulated using *LOAD BLAST

ENHENCED keyword, assuming 260 g TNT detonates directly above the centre of the panel at a 650 mm standoff distance measured from the back flat sheet centre point. The material model incorporating strain rate effect, i.e. Cowper-Symonds model is used. The material properties are the same as the ones in the model calibration given in Table 1. The peak reaction forces at the panel boundaries are calculated as the peak value of the sum of the nodal forces on each edge by defining the keywords *SET NODE OPTION and *DATABASE NODAL FORCE GROUP.

3.3 Results and Discussions

Table 3. Peak displacements, internal energy, boundary reaction forces of four forms of panels

Category	Layer thickness (mm)			Energy absorption by Core (kJ)	Peak displacement at centre of back plate (mm)	Peak boundary reaction force (10^5 N)		
	Top	Core	Back			F_x	F_y	$F_{vertical}$
F1	-	-	5	-	21.7	6.05	6.07	2.31
A5-H50	2	1.29	1.5	1.47	15.4	2.72	1.51	1.36
S5-H50	2	1.53	1.5	0.24	13.9	1.57	1.65	1.60
D5-H50	2	1.20	1.5	1.02	14.2	1.81	1.81	0.71

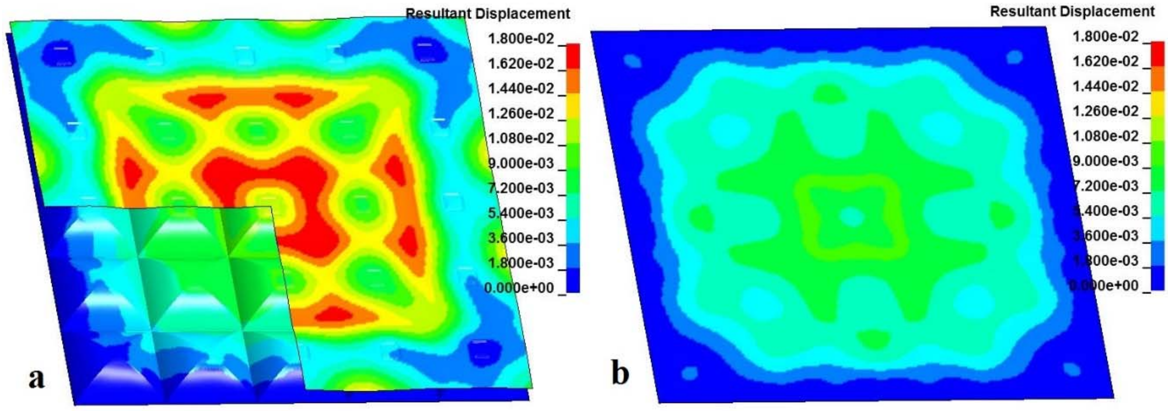

Figure 9. Contour of resultant displacement of D5-H50 square dome panel (a) Top layer and core, (b) Back layer, Unit: meter

Peak displacement contour plots of both the top and back plates of the D5-H50 panel are shown in Figure 9. Time history curves of displacement at the centre of back plate are shown in Figure

10. The structural responses of the panels including peak displacement, internal energy absorption of the top and back layers and peak boundary reaction forces are calculated and given in Table 3. To keep the total mass of each panel the same, the thicknesses of layers of each panel are calculated as given in Table 3 with a constant 2 mm and 1.5 mm thickness for the top and back layer respectively, and varying thickness for the core. The numerical results show that the peak displacements at the centre point of load-self-cancelling structures i.e. A5-H50, S5-H50 and D5-H50 are reduced to 15.4 mm, 13.9 mm and 14.2 mm respectively as compared to the peak displacement of 21.7 mm of the flat plate. As shown, the S5-H50 yields the smallest peak displacement among these panels, followed by D5-H50. This is because S5 and D5 with two-way symmetry of unit cells results in a stiffer structure to deform comparing with the uni-directional multi-arch panel A5-H50, as can be seen in Figure 10 (a) where the vibration periods of S5 and D5 are much smaller than F1 and A5. The arches as shown in Figure 6 can deform much more easily along the x-axis than the y-axis because of the configuration of uni-directional arch. This can also been seen from the internal energy absorption of the core, where the A5-H50 holds a much higher value than the other two types. Furthermore, S5-H50 has a thicker core than the other two panels, resulting in the smallest peak displacement at centre of the back plate.

As the numerical models including blast loading, boundary conditions, and geometries are symmetrical, the reaction forces F_x and F_y are taken as the sum of nodal forces on one edge only. F_z is the vertical reaction force which is taken as the sum of nodal forces in Z direction on all of four edges. Figure 11 shows the peak values of boundary reaction forces in three directions of four panels. Due to the geometrical symmetry of the panel F1, S5 and D5, the peak reaction forces along X and Y directions are very close in value. As given in Table 3, the reaction forces of A5-H50 uni-directional LSC structure in X and Y directions are 272 kN and 151 kN, respectively, which are around 55% and 75% less than the baseline F1 flat plate. The boundary reaction force in vertical directional is reduced by 41.1% to 160 kN. S5-H50 shows a similar LSC capacity, with a 72.7% reduction of boundary reaction forces in the in-plane directions and 30.7% reduction in the out-of-plane direction as compared to the flat plate F1. D5-H50 shows a more significant reduction with the reaction forces in the out-of-plane direction reducing to 71 kN, which is around 69.3% less than that of F1. The bi-directional LSC square dome panel (D5) achieves further 47.8% reduction in the out-of-plane boundary reaction force of the multi-arch structure (A5) and 55.6% less than that of the grid sphere dome (S5). These observations indicate the bi-directional square dome panel (D5) performs the best in cancelling blast loads, since the out-of-plane boundary reaction force of D5 is the smallest.

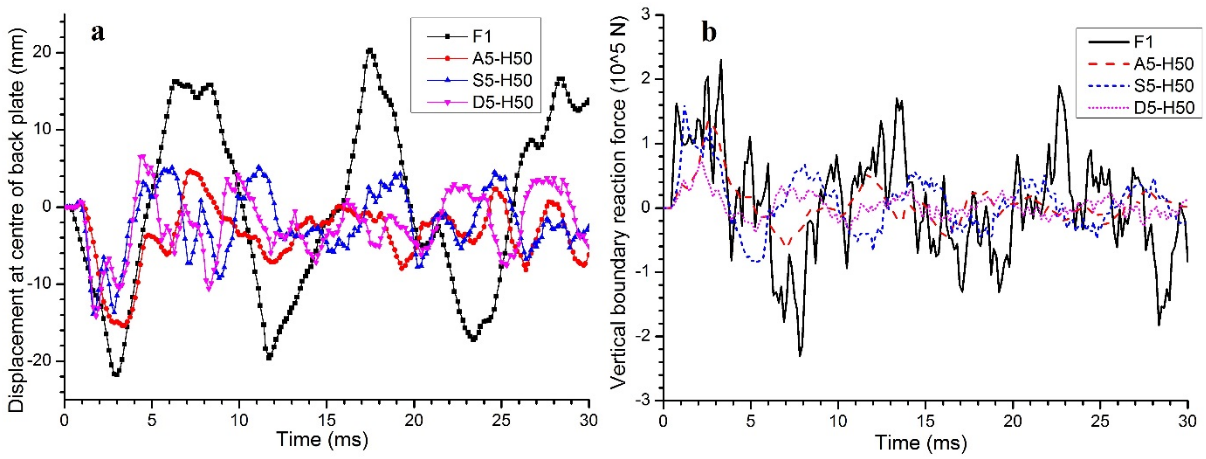

Figure 10. (a) Displacement time histories of centre point on back plate for four panels; (b) Time histories of vertical boundary reaction forces for four panels

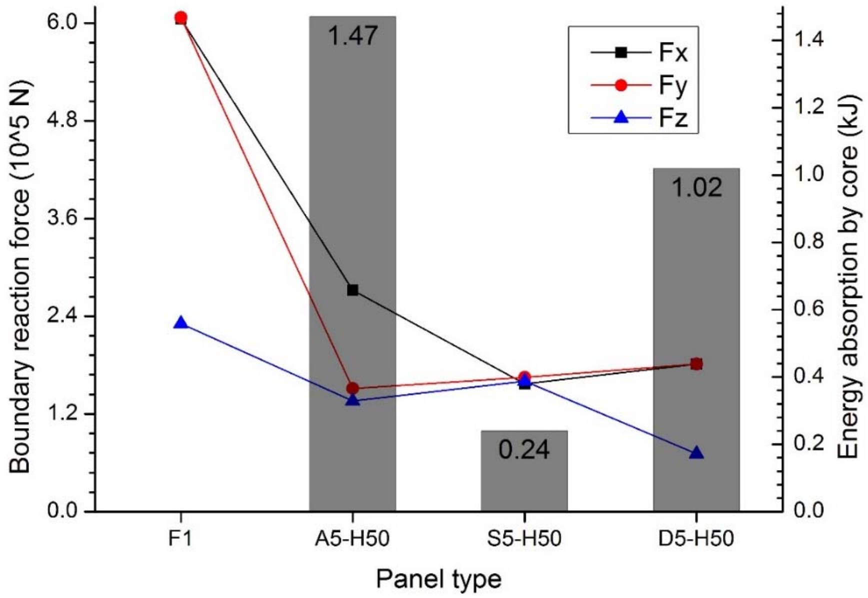

Figure 11 Boundary reaction forces in X, Y, Z directions and energy absorption by the core of four types of panels

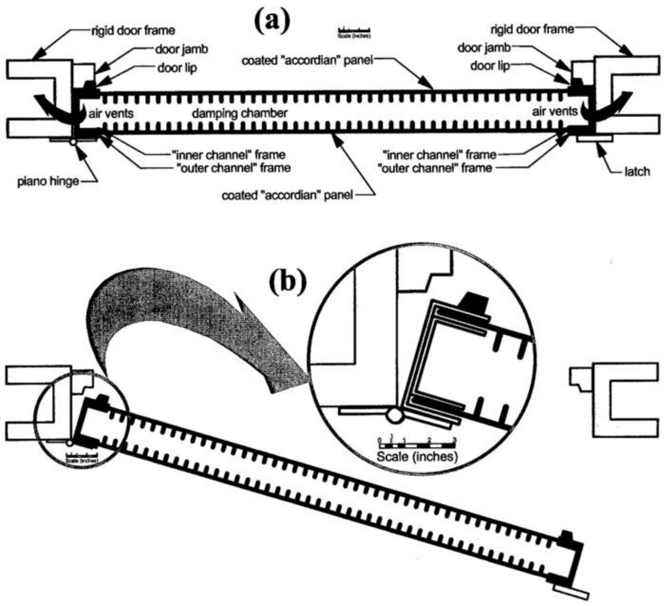

Figure 12. Schematic diagram of a typical blast resistant door panel [35]

It is worth noting that the boundary reaction force in out-of-plane direction is the most critical among those in three principal directions for many blast resistance applications such as blast resistant door, shield and sacrificial cladding, where the panels are simply supported at the boundary or placed directly on top of the protected structure. An example of blast resistant door is shown in Figure 12. Under blast loading, the door panel tends to bend inwards with reaction force exerting on the door frame mostly in the out-of-plane direction rather than the in-plane directions. The load-self-cancelling mechanism is shown in Figure 13. The blast loading with extremely short duration (less than 1 ms in this study) is applied onto the front plate. The loading is then transmitted along the arch and to the intersections of the arches where partial of the loading is cancelled out by adjacent arches before it reaches the panel supports. Therefore it reduces the loading transmitted to the back plate and support in the out-of-plane direction. All LSC structures (A5, S5 and D5) cancelling out partial blast loading at the intersections of arches or domes, lead to less blast loads being transmitted to the support. The longer and more evenly spread out of the intersections between arches or domes can lead to a higher LSC capacity, therefore the square dome panel (D5) has higher efficiency in reducing vertical boundary reaction force than the sphere domes (S5), in which the intersections between adjacent unit cells are points instead of lines.

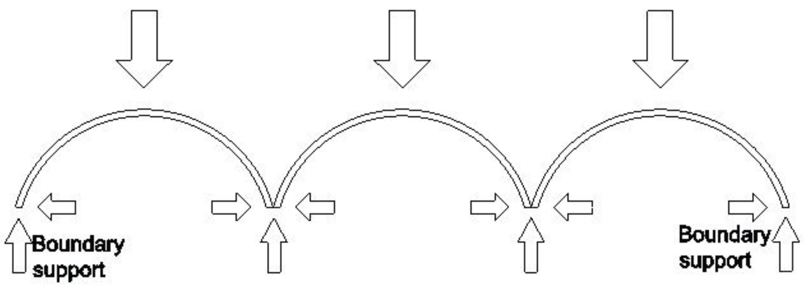

Figure 13. Schematic diagram of load-self-cancelling mechanism using arch or dome structure

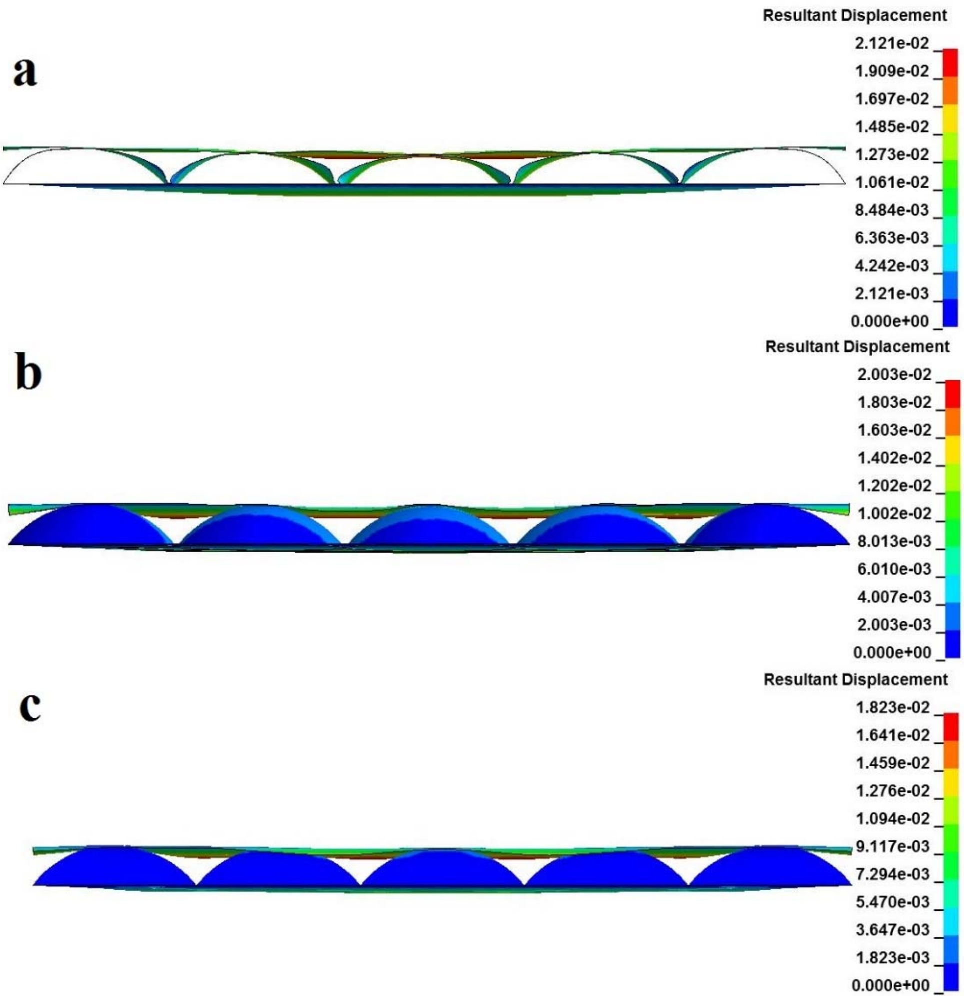

Figure 14. Front view of three panels' contour plots at their maximum back plate centre displacements (a) A5-H50; (b) S5-H50; (c) D5-H50; unit: meter

Figure 14 shows the deformation mode of three LSC panels at their maximum displacement level. The uni-directional multi-arch panel (A5) has the largest displacement for both the top plate and the core, obvious bending deformation can be spotted for the individual arch especially those at the middle of the panel. The bi-directional LSC panels (S5 and D5) show a different damage mode due to the increase in crushing resistance of individual unit. The peak displacement at the back face plate is smaller and the individual unit cell is more intact. This can be also confirmed from the energy absorption by the core listed in Table 3, where the core of A5 absorbs more energy than the core of the other two panels (S5 and D5), indicating larger plastic deformation of the core. With a 25% thicker wall of the core, S5 shows a slightly lower peak displacement of the back plate and a smaller energy absorption than the square dome panel D5. However, the square dome panel (D5) has better performance in terms of reducing vertical boundary reaction force than the sphere domes (S5).

4. Parametric Studies

In this section, performances of the LSC square dome panels with different configurations and parameters are investigated to evaluate their blast resistance capacities. These parameters include the number of square dome, dome height, layer material. Unless otherwise noted, the panel considered is 1 m by 1 m with 50 mm arch height subjected to 260 g of TNT equivalency detonated at 650 mm directly above the centre point of back flat layer, which is the same as the previous section. The top and back layer thickness is kept constant while the thickness of the core is varied in order to maintain the same overall mass of the panels. To examine the performances, the peak displacement, internal energy absorption and peak boundary reaction forces are extracted and compared.

4.1 Effect of dome number

The panels with different numbers of square domes are discussed in this section. D3, D4, D5, D6 and D7 represent the number of domes along one horizontal direction, therefore the total numbers of domes for these panels are 9, 16, 25, 36 and 49, respectively, as listed in Table 4. The results indicate that in general the peak deflection at the centre of the back layer decreases with the increase in the number of domes, except the panel D4 and D6. This is because more dome numbers lead to more connections between the layers. The panel thus becomes stiffer to bend, even though the thickness of the core decreases slightly with the increasing dome number. The displacement time histories of the panels are shown in Figure 15.

Table 4. Peak displacements, internal energy, boundary reaction forces of square dome panels with varying dome numbers

Category	Layer thickness (mm)			Energy absorption by core (kJ)	Peak displacement at centre of back plate (mm)	Peak boundary reaction force (10^5 N)		
	Top	Core	Back			F_x	F_y	F_z
D3-H50	2	1.38	1.5	1.22	21.3	1.39	1.4	0.88
D4-H50	2	1.29	1.5	1.12	12.2	2.13	2.13	0.75
D5-H50	2	1.20	1.5	1.02	14.2	1.81	1.81	0.71
D6-H50	2	1.10	1.5	1.16	9.6	2.10	2.10	0.70
D7-H50	2	1.01	1.5	1.29	10.1	2.10	2.11	0.71

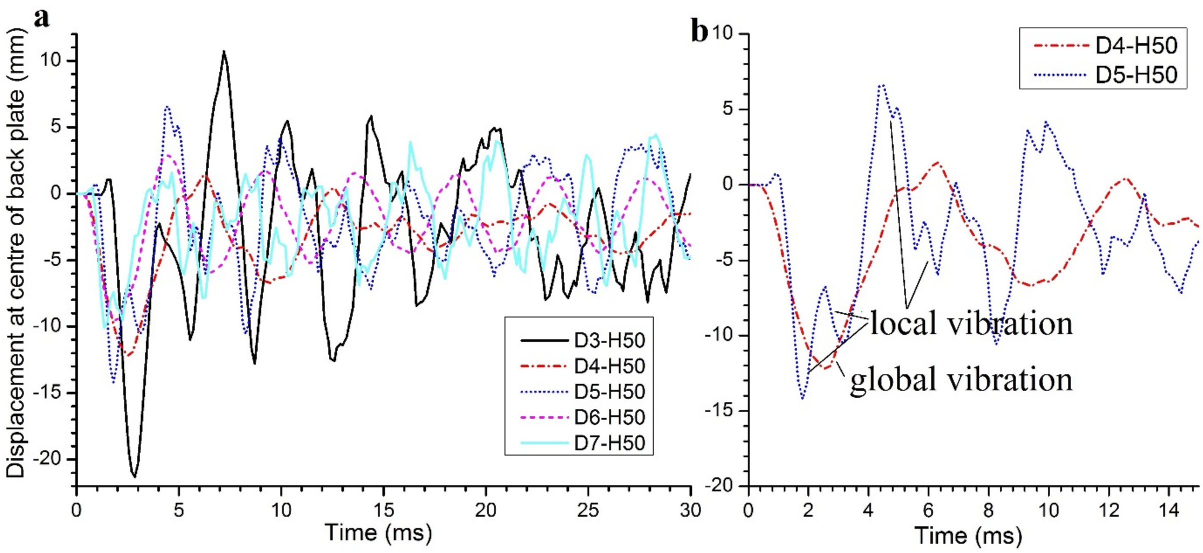

Figure 15. Displacement time histories of centre point of the back plate (a) for the panels with different dome numbers; (b) zoomed in for D4-H50 and D5-H50

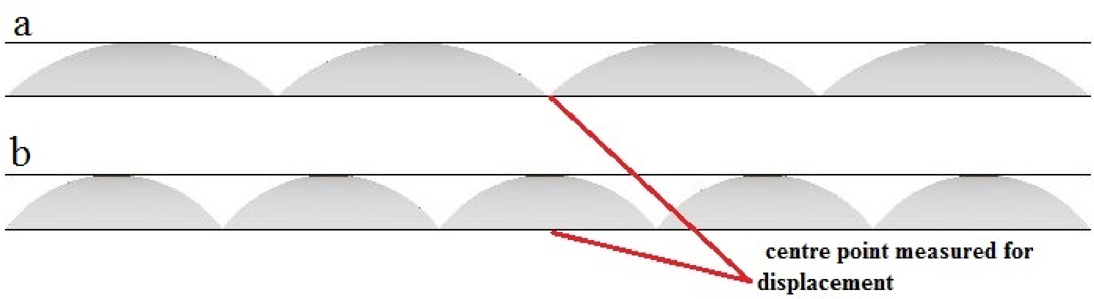

Figure 16. Illustration of the centre point location relative to the dome core connections (a) even and (b) odd number of square domes

The panels with an even number of dome core, i.e., D4 and D6, show smaller deformation at the centre point of the back layer as compared to those with odd number of dome core, because the centre point locates at the interactions between the adjacent domes as shown in Figure 16. Because four adjacent domes intersects at the centre point, which makes the local stiffness of the point high, therefore leads to relatively smaller deformation of the point. Whereas the centre point of the panel with odd number of dome core locates at the centre of a dome, hence there is no local stiffening effect at the point. Moreover, after short duration of blast loading (less than 1ms in this study), free vibration occurs. As shown in Figure 15, only global vibration of the back plate contributes to the centre point displacement response when the core has an even number of domes, but both the global response and local response modes, i.e., vibration modes between intersection points, contribute to the displacement responses of the centre point when the core has an odd number of domes. These are the reasons why the centre point of panels with odd number of domes experiences relatively smaller deformations. Nonetheless increasing the number of domes makes the panel stiffer and hence reduces the global panel deformations.

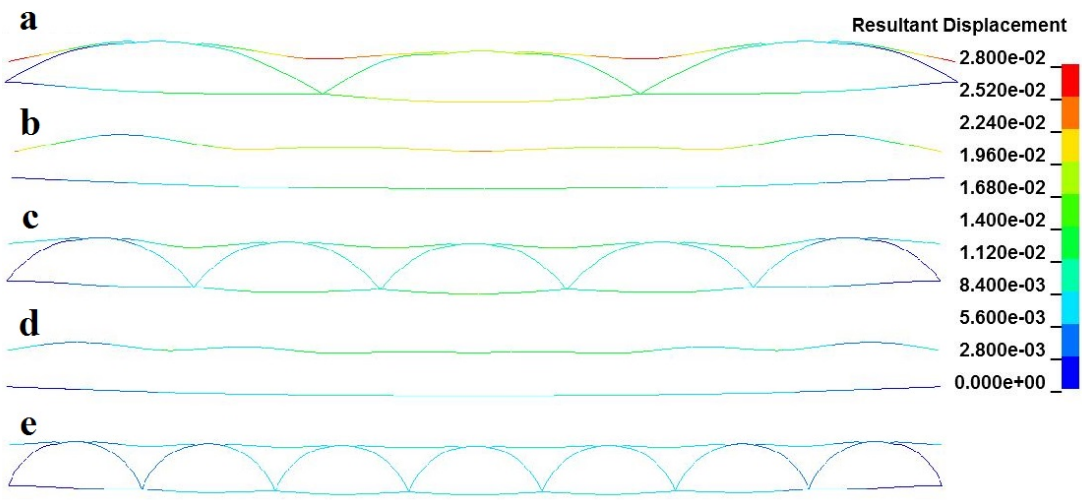

Figure 17. Middle plane cross-section views of square dome panels at their peak back plate centre deflection, (a) D3-H50; (b) D4-H50; (c) D5-H50; (d) D6-H50; (e) D7-H50; units: meter,

note domes are not cut through for (b) and (d) where the centre planes are located at the intersection of domes, only top and back plates are shown

The cross-section view of deformation modes of the panels are shown in Figure 17. The peak boundary reaction forces for D4 to D7 along the both in-plane directions are similar in value, as given in Table 4 and Figure 18. D3 square dome panel has the lowest peak boundary reaction forces in the in-plane directions among these panels. This might be caused by the large deformation and energy absorption of the top plate and the core as shown in Figure 17 (a). Since the peak reaction force in the out-of-plane direction is more critical in the design as discussed above, it is of more interests in this study. As shown, the peak out-of-plane reaction force decreases around 20.5% to 70 kN with the increasing number of domes from D3 to D6, but increases slightly to 71 kN from D6 to D7. As explained in the previous sections regarding the mechanism of using arch for load-self-cancelling, the more uniformly distributed loads on the adjacent domes increase the effectiveness of cancellation and decrease the peak reaction forces at the boundaries of panels. With the increasing number of square domes, the load can be distributed more evenly onto the adjacent domes, resulting in a better LSC performance. However, further increasing the number of domes cannot lead to more effective load-self-cancelling of the panel. As the dome height is set to be fixed, with the increasing number of domes, the arches of domes are becoming closer to a half circle shape as shown in Figure 17. The loads transferred to the intersections of the arches decreases, which leads to a reduction in load cancellation. Another reason is that increasing the number of domes increases the surface area of core, and its thickness has to be thinned to maintain the same overall mass, which might decrease the bending stiffness of the whole panel. It can be concluded that increasing the number of square domes lowers the boundary reaction forces in the out-of-plane direction. However, this trend is no longer true when the dome base dimension approaches to the dome height, i.e., the dome shape approaches to a semi sphere. Among the configurations considered in the present study, D6-H50 has the best performance, with the smallest peak displacement at the back face and the smallest out-of-plane peak reaction force.

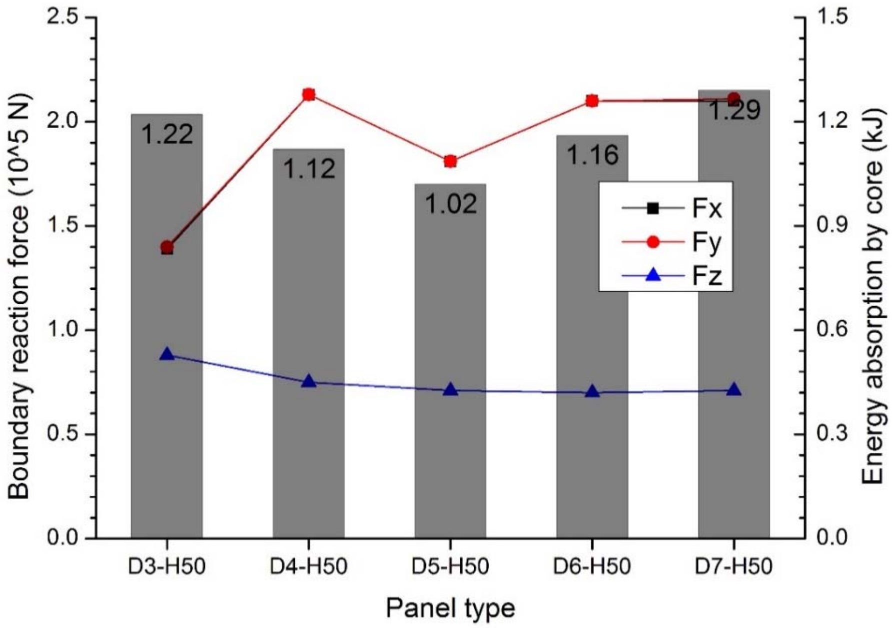

Figure 18. Boundary reaction forces in X, Y, Z directions and energy absorption by core of panels with varying numbers of square domes

4.2 Effect of dome height

In this section, the effect of dome height is investigated. The dome height varies from 30 mm to 70 mm with 10 mm interval. The peak responses of the panels are given in Table 5, and illustrated in Figure 19. It is found that the peak displacement at the back decreases with the increasing height of the domes even though the blast load acting on the panel increases owing to the reduced stand-off distance from the explosion centre to the panel. The panel D5-H30 has a similar peak displacement as the baseline F1 flat plate (i.e. 21.9 mm). A relatively limited load-self-cancelling effect can be observed when comparing with other square dome structures. As compared with F1, the peak displacement of square dome panel reduces by 25%, 32%, 35%, 37% and 39% for the panels with different dome heights varying from 30 mm to 70 mm, respectively. This is because the bending stiffness of the panel increases with the height of the domes.

Table 5. Peak displacements, internal energy, boundary reaction forces of square dome panels with varying heights

Category	Layer thickness (mm)			Energy absorption by core (kJ)	Peak displacement at centre of back plate (mm)	Peak boundary reaction force (10^5 N)		
	Top	Core	Back			F_x	F_y	F_z
D5-H30	2	1.41	1.5	0.83	16.2	2.36	2.36	0.73
D5-H40	2	1.34	1.5	0.91	14.7	1.88	1.88	0.73
D5-H50	2	1.20	1.5	1.02	14.2	1.81	1.81	0.71
D5-H60	2	1.10	1.5	1.12	13.6	1.40	1.40	0.66
D5-H70	2	1.01	1.5	1.43	13.3	1.12	1.11	0.69

The peak values of boundary reaction forces also decrease with the increase in the dome height from 30 mm to 60 mm. However further increase the dome height to 70 mm leads to a slight increase in the boundary reaction forces in the out-of-plane direction as compared with D5-H60. This again can be explained by the dome geometries. The angle of dome at intersection edge can be calculated as 53 degree, 62 degree and 70 degree for the panel D5-H50, D5-H60 and D5-H70, respectively. The highest dome H70 has the largest angle at the intersection, which leads to less effective load cancelling performance. Similar to the results presented in Section 4.1, the more critical vertical component of boundary reaction force first decreases and then increases slightly with the increasing number of domes, which is also associated with the change of the angle at dome intersections. Moreover, the LSC panels with higher domes experience higher overpressure due to the reduction of the distance from the front plate to the detonation. Furthermore, the panels with higher domes have a larger surface area of the dome shaped layer, which leads to a reduction on the thickness of the core. These combined factors affect the LSC capacity of the structure. Similarly, the energy absorption by the core increases with the rising height of the core as shown in Figure 19. With higher cores, the bending stiffness of the panel is higher, but the crushing of each individual dome becomes easier due to thinner dome wall thickness and larger crushing distance. Therefore, less bending of the panel but more deformation of the core is observed for the panels with higher domes. It is found that D5-H60 performs the best among the panels considered in the present study in terms of the effectiveness of load-self-cancelling of the structure using the out-of-plane peak reaction force as criteria.

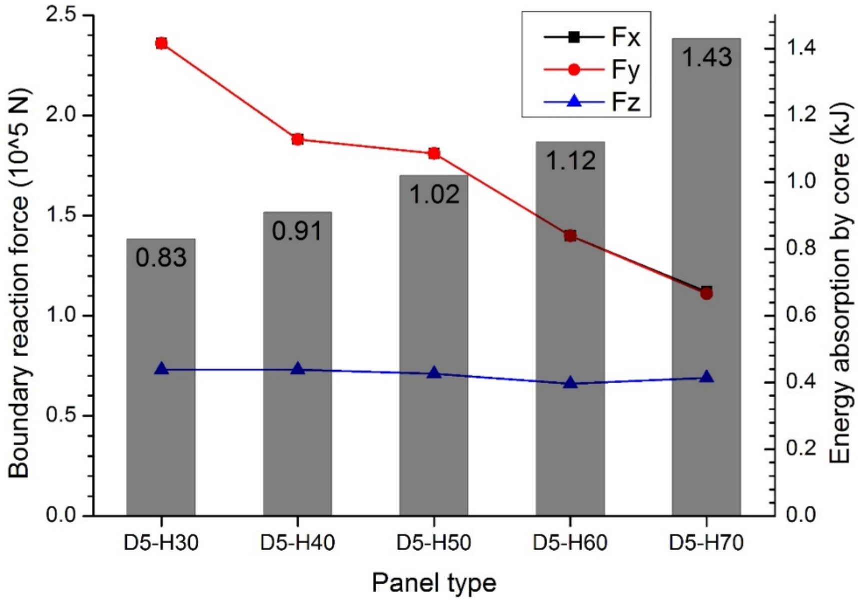

Figure 19. Boundary reaction forces in X, Y, Z directions and energy absorption by the core of panels with varying heights of square domes

4.3 Effect of blast intensity

Four levels of blast intensities are considered in this section. Four TNT weights of 260 g, 0.5 kg, 1 kg and 4 kg are set to examine blast resistance capacity of the proposed bi-directional LSC panel. Scaled distance is calculated based on the equation (3) and listed with structural responses in

Table 6. Peak reflected pressure and positive phase impulse exerted on the front plate are calculated based on the centre element of the panel. The peak displacement, boundary reaction forces on the three axes increase with the increment of blast intensity as expected. Increasing trend of energy absorption by the core with the increase of blast intensities can be observed as well.

Table 6. Peak displacements, internal energy, boundary reaction forces of square dome panels under different blast intensities

Category	Scaled distance ($m/kg^{1/3}$)	Peak reflected pressure at centre (MPa)	Positive phase impulse (Ns)	Energy absorption by core (kJ)	Peak displacement at centre of back plate (mm)	Peak boundary reaction force (10^5 N)		
						F_x	F_y	F_z
D5-H50-0.26kg	0.94	5.8	389	1.02	14.2	1.81	1.81	0.71
D5-H50-0.5kg	0.76	10.4	646	3.04	21.8	1.98	1.95	1.35
D5-H50-1kg	0.60	18.4	1096	8.67	46.1	4.94	4.95	3.23
D5-H50-4kg	0.38	50.7	3448	51.7	146	8.39	8.39	11.7

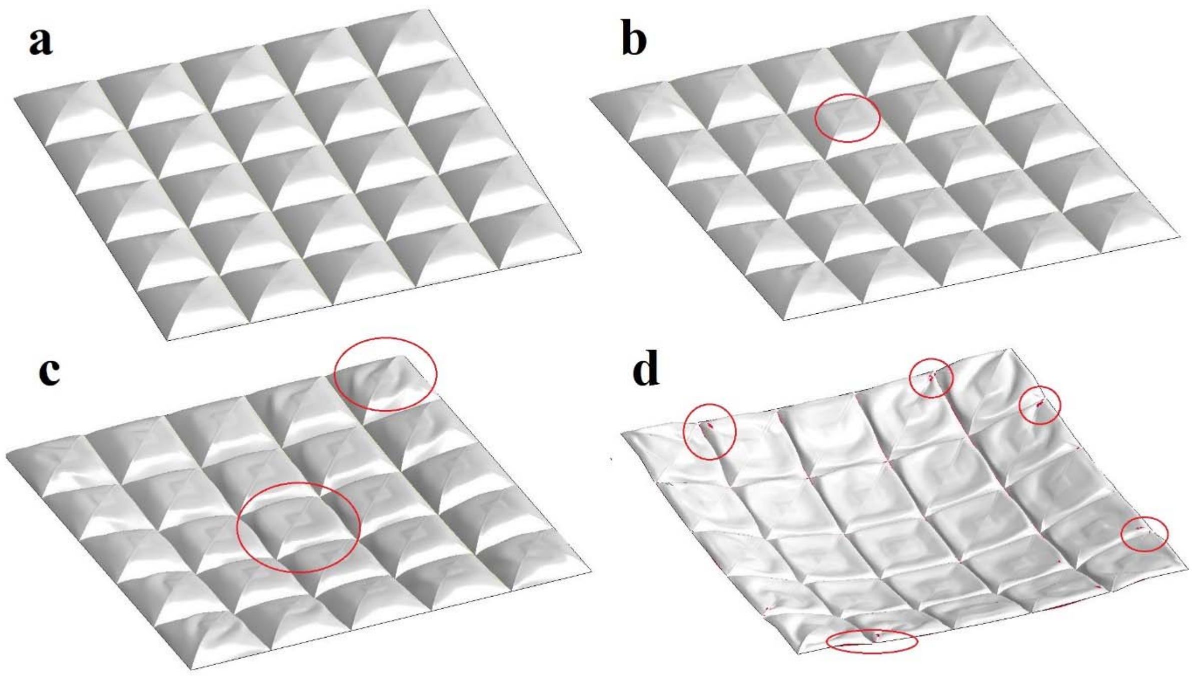

Figure 20. Damage modes of (a) D5-H50-0.26kg; (b) D5-H50-0.5kg; (c) D5-H50-1kg; (d) D5-H50-4kg at their maximum deflections, top plate removed for illustration

Damage modes of square dome panel under different blast intensities are shown in Figure 20. Both global damage of the panel and localized damage of individual square dome can be observed for the cases with higher blast intensities. For D5-H50-0.26kg and D5-H50-0.5kg, only slight global deformation of the panels can be observed. The panel subjected to the blast loads from the other two cases experience severe localized damage of individual square domes at the centre and corners, as well as global deformation. The localized deformation near the corner under 4kg detonation (Figure 20 d) is caused by the global deformation of the panel when the panel bends along the both in-plane directions. All the domes are crushed under blast load from 4 kg explosion, tearing and breakage of the panel appear near the corners of some individual domes as shown in Figure 20 (d) marked in red circles. The plastic strain of back plate under blast loading of 4kg explosion is shown in Figure 21, where high plastic strain of elements at the outer edges and intersections of domes are captured. The line of elements at the outer edges are eroded due to stress concentration as circled in red. An increase in the damage of individual square domes and the whole panel can be observed with the increase of blast intensity.

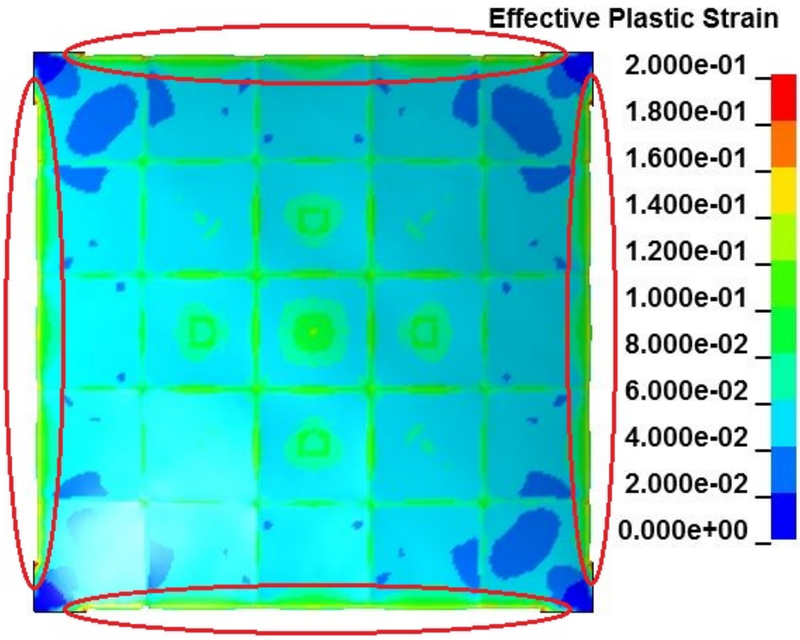

Figure 21. Plastic strain of back flat plate of D5-H50-4kg, eroded edge elements are circled in red

4.4 Effect of different materials

The layers made of different materials are considered in this section. Aluminium alloy Al-2024-T3 is used to replace the core made of steel. Since aluminium alloy shows less evident strain rate effect [13], strain rate effect is not considered in the material model and the rest of the parameters used in the material model are given in

Table 7.

Table 7. Material properties of Aluminium alloy Al-2024-T3 [13]

Property	**Young's modulus (GPa)**	**Poisson's ratio**	**Yield stress (MPa)**	**Tangent modulus (MPa)**	**Density (kg/m^3)**
Value	72	0.33	318	737	2680

Structural responses are summarized in Table 8 and shown in Figure 22 and Figure 23. The centre point peak deflection of back layer increases from 14.2 mm to 16.5 mm by replacing steel with aluminium alloy core. Similarly, the internal energy absorption of the core made of aluminium alloy increases 70.6% and the internal energy absorption of back flat layer increases as well. It is found that the out-of-plane boundary reaction forces increase 42.3% by using aluminium alloy core. It is because Aluminium alloy is less stiff than steel and it is easier to deform under the same load, which reduces the load-self-cancelling capability.

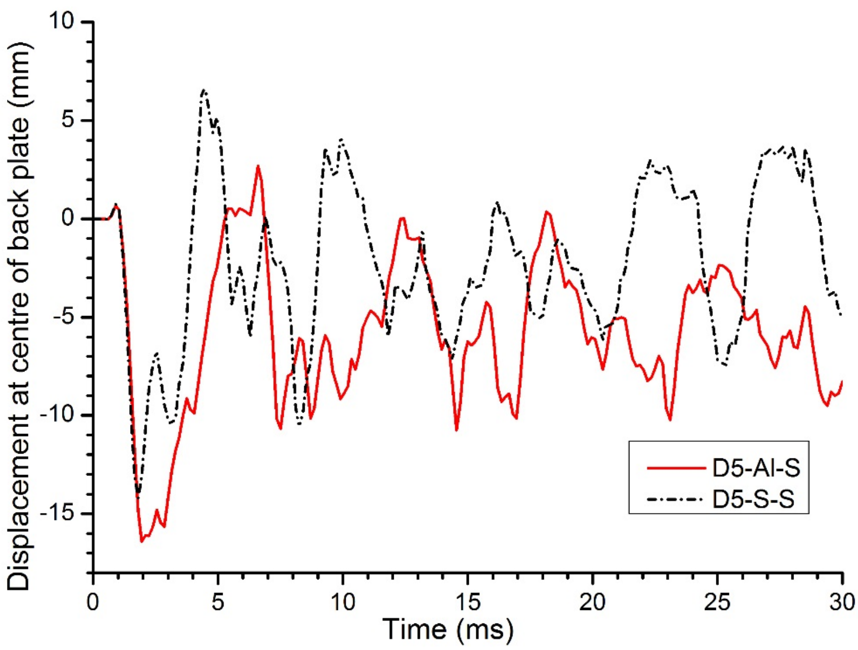

Figure 22. Displacement history of centre point on back plate for panel with different core materials

Table 8. Peak displacements, internal energy, boundary reaction forces of square dome panels with different core materials

Category	Layer thickness (mm)			Energy absorption by core (kJ)	Peak displacement at centre of back plate (mm)	Peak boundary reaction force (10^5 N)		
	Top	Core	Back			F_x	F_y	F_z
D5-S-S	2 (steel)	1.2 (steel)	2.5 (steel)	1.02	14.2	1.81	1.81	0.71
D5-Al-S	2 (steel)	1.2 (Al)	2.5 (steel)	1.80	16.5	1.39	1.39	1.01

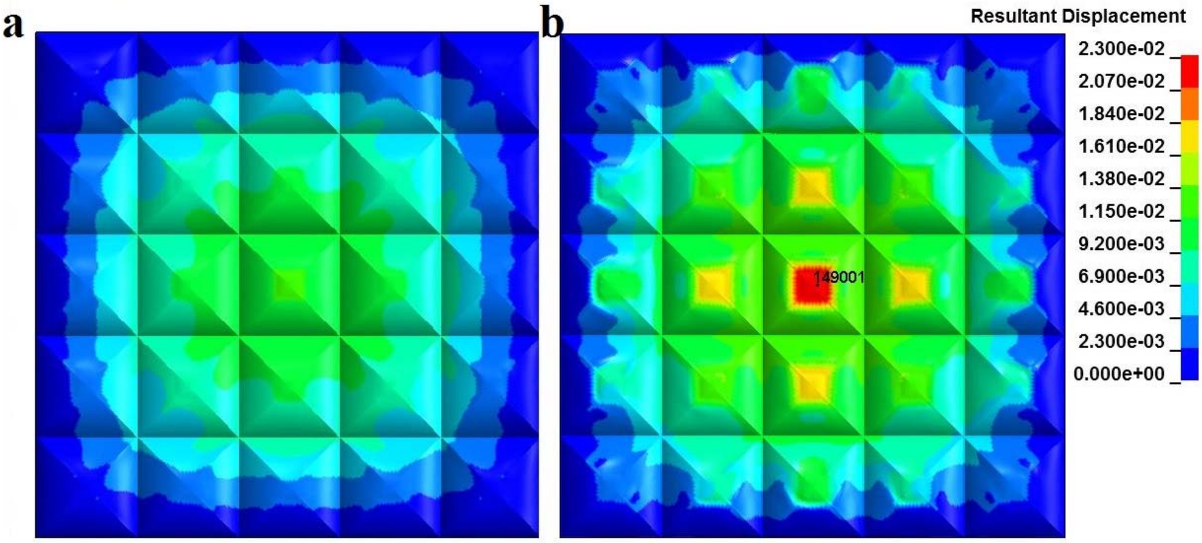

Figure 23. Contour plots of resultant displacement of D5-H50 square dome panel (a) with steel core, (b) with aluminium core, Unit: meter

Energy absorption is usually achieved by plastic deformation [8], fracture and friction of structure [36] during blast or impact event. In this study, the load-self-cancelling structure is functioned by the arching geometry of the structure and stress propagation after the loading. The excessive deformation of the core leads to the change of arch shape, which might undermine load-self-cancelling capability. As illustrated in Figure 23, the panel with aluminium core experiences a much more severe deformation than the one with steel core. Hence, the locations with stress concentration and large deformation are suggested to be strengthened to maintain load-self-cancelling function by using stiffer material or stiffened structure such as stiffened multi-arch double layer panels [30].

5. Conclusion

A bi-directional load-self-cancelling (LSC) square dome sandwich panel is proposed in this study and its blast LSC effectiveness is numerically demonstrated in the most critical direction (i.e. out-of-plane direction), after comparing with the flat plate, uni-directional LSC multi-arch structure and sphere dome structure of the same mass. Up to around 69% reduction in boundary reaction force is observed as compared with the flat panel. Parametric studies on the number of square domes, dome height, blast intensity and material are also carried out. It is found that the panel with more numbers of domes and stiffer domes has better load-self-cancelling capability. Blast resistance capacity of the panel also enhances with the increase of dome height. However, further increasing the number and height of domes may reduce the blast resistance performance of the panel. This new structural form might find applications to fabrication of sandwich panels to resist blast loadings.

6. Acknowledgements

The authors acknowledge the support from Australian Research Council via Discovery Early Career Researcher Award (DE160101116).

7. References

[1] U. DoS, Country reports on Terrorism 2012, Bureau of Counterterrorism, US DoS, 2013.
[2] H. Hao, Predictions of Structural Response to Dynamic Loads of Different Loading Rates, International Journal of Protective structures, 6, 2015, 585-605.
[3] H. Hao, Y. Hao, J. Li, W. Chen, Review of the current practices in blast-resistant analysis and design of concrete structures, Adv. Struct. Eng, 19, 2016, 1193-1223.
[4] A. Alghamdi, Collapsible impact energy absorbers: an overview, Thin-walled structures, 39, 2001, 189-213.
[5] Y. Wang, J.Y.R. Liew, Blast performance of water tank with energy absorbing support, Thin-Walled Structures, 96, 2015, 1-10.
[6] Y. Wang, H. Zhou, Numerical study of water tank under blast loading, Thin-Walled Structures, 90, 2015, 42-48.
[7] W. Chen, H. Hao, Numerical study of a new multi-arch double-layered blast-resistance door panel, International Journal of Impact Engineering, 43, 2012, 16-28.

[8] G. Lu, T. Yu, Energy Absorption of Structures and Materials, Woodhead publishing limited, Cambridge England, 2003.
[9] F. Zhu, G. Lu, A review of blast and impact of metallic and sandwich structures, EJSE Special Issue: Loading on Structures, 2007.
[10] F. Zhu, G. Lu, D. Ruan, Z. Wang, Plastic deformation, failure and energy absorption of sandwich structures with metallic cellular cores, International Journal of Protective structures, 1, 2010, 507-541.
[11] S.C.K. Yuen, G. Nurick, The Use of Tubular Structures as Cores for Sandwich Panels Subjected to Dynamic and Blast Loading: A Current "State of the Art", in: Blast Mitigation, Springer, 2014, pp. 229-248.
[12] D.D. Radford, G.J. McShane, V.S. Deshpande, N.A. Fleck, The response of clamped sandwich plates with metallic foam cores to simulated blast loading, International Journal of Solids and Structures, 43, 2006, 2243-2259.
[13] F. Zhu, L. Zhao, G. Lu, Z. Wang, Structural response and energy absorption of sandwich panels with an aluminium foam core under blast loading, Advances in Structural Engineering, 11, 2008, 525-536.
[14] L. Jing, Z. Wang, L. Zhao, The dynamic response of sandwich panels with cellular metal cores to localized impulsive loading, Composites Part B: Engineering, 94, 2016, 52-63.
[15] N. Gardner, E. Wang, A. Shukla, Performance of functionally graded sandwich composite beams under shock wave loading, Composite Structures, 94, 2012, 1755-1770.
[16] X.R. Liu, X.G. Tian, T.J. Lu, B. Liang, Sandwich plates with functionally graded metallic foam cores subjected to air blast loading, International Journal of Mechanical Sciences, 84, 2014, 61-72.
[17] L. Zhang, R. Hebert, J.T. Wright, A. Shukla, J.-H. Kim, Dynamic response of corrugated sandwich steel plates with graded cores, International Journal of Impact Engineering, 65, 2014, 185-194.
[18] A. Hanssen, L. Enstock, M. Langseth, Close-range blast loading of aluminium foam panels, International Journal of Impact Engineering, 27, 2002, 593-618.
[19] P. Jasion, E. Magnucka-Blandzi, W. Szyc, K. Magnucki, Global and local buckling of sandwich circular and beam-rectangular plates with metal foam core, Thin-Walled Structures, 61, 2012, 154-161.
[20] G. Imbalzano, P. Tran, T.D. Ngo, P.V.S. Lee, A numerical study of auxetic composite panels under blast loadings, Composite Structures, 135, 2016, 339-352.
[21] I. Maskery, A. Hussey, A. Panesar, A. Aremu, C. Tuck, I. Ashcroft, R. Hague, An investigation into reinforced and functionally graded lattice structures, Journal of Cellular Plastics, 2016.
[22] S. Li, S. Zhao, W. Hou, C. Teng, Y. Hao, Y. Li, R. Yang, R.D.K. Misra, Functionally Graded Ti-6Al-4V Meshes with High Strength and Energy Absorption, Advanced Engineering Materials, 18, 2016, 34-38.
[23] S.H. Yoo, S.H. Chang, M.P.F. Sutcliffe, Compressive characteristics of foam-filled composite egg-box sandwich panels as energy absorbing structures, Composites Part A: Applied Science and Manufacturing, 41, 2010, 427-434.
[24] M. Zupan, C. Chen, N.A. Fleck, The plastic collapse and energy absorption capacity of egg-box panels, International Journal of Mechanical Sciences, 45, 2003, 851-871.
[25] L. Jing, C. Xi, Z. Wang, L. Zhao, Energy absorption and failure mechanism of metallic cylindrical sandwich shells under impact loading, Materials & Design, 52, 2013, 470-480.
[26] L. Jing, Z. Wang, L. Zhao, Response of metallic cylindrical sandwich shells subjected to projectile impact—Experimental investigations, Composite Structures, 107, 2014, 36-47.
[27] J. Shen, G. Lu, Z. Wang, L. Zhao, Experiments on curved sandwich panels under blast loading, International Journal of Impact Engineering, 37, 2010, 960-970.

[28] J. Shen, G. Lu, L. Zhao, Z. Qu, Response of Curved Sandwich Panels Subjected to Blast Loading, Journal of Performance of Constructed Facilities, 25, 2011, 382-393.
[29] W. Chen, H. Hao, Experimental investigations and numerical simulations of multi-arch double-layered panels under uniform impulsive loadings, International Journal of Impact Engineering, 63, 2014, 140-157.
[30] W. Chen, H. Hao, Numerical simulations of stiffened multi-arch double-layered panels subjected to blast loading, International Journal of Protective Structures, 4, 2013, 163-188.
[31] T. Yu, X. Tao, P. Xue, The energy-absorbing capacity of grid-domed textile composites, Composites science and technology, 60, 2000, 785-800.
[32] S.D. Boyd, Acceleration of a plate subject to explosive blast loading-trial results, in, DTIC Document, 2000.
[33] J.O. Hallquist, LS-DYNA theory manual, Livermore software Technology corporation, 3, 2006, 25-31.
[34] J.O. Hallquist, LS-DYNA keyword user's manual, Livermore Software Technology Corporation, 970, 2007.
[35] M. Anderson, D. Dover, Lightweight, blast-resistant doors for retrofit protection against the terrorist threat, in, Applied Research Associates Inc Panama City FL, 2003.
[36] W. Chen, H. Hao, Numerical Study of Blast-Resistant Sandwich Panels with Rotational Friction Dampers, International Journal of Structural Stability and Dynamics, 13, 2013, 1350014.